RSC Advances

PAPER

View Article Online
View Journal | View Issue

Cite this: *RSC Adv.*, 2024, **14**, 16828

Polyvinylidene fluoride/graphene oxide/polyimide composite high-efficiency $PM_{2.5}$ filtration nanofiber membranes

Hangdong Chen,[a] Xun Sun,[b] Ying Wang,[c] Lixian Shi,[d] Xuan Liu *[a] and Nantao Hu *[e]

Received 19th March 2024
Accepted 1st May 2024

DOI: 10.1039/d4ra02064b

rsc.li/rsc-advances

Particulate air pollution is a global environmental problem, with $PM_{2.5}$ being the primary pollutant. One of the most effective ways to remove particles from the air is through filtration. Therefore, high-performance air filters are urgently needed to combat the harm caused by $PM_{2.5}$. This study uses an electrospinning technique to prepare high-efficiency polyvinylidene fluoride/graphene oxide/polyimide nanofiber membranes. These composite nanofiber membranes demonstrate high filtration efficiency (99.6%), low pressure drop (123 Pa), remarkable thermal stability (450 °C), and excellent mechanical strength (7 MPa). Considering the advantages, these highly efficient nanofiber membranes can find advanced applications in industrial and civil infrastructures.

1. Introduction

Particulate air pollution is a global environmental issue, with continuous exposure leading to irreparable risks.[1] Major air pollutants include micro-scale airborne particulate matter ($PM_{2.5}$ as well as PM_{10}) and hazardous gases in the form of aerosols (such as SO_2, CO, NO_2, and O_3). These pollutants are mainly produced by steel mills, power plants, the cement industry, and vehicles' combustion of fossil fuels.[2,3] Atmospheric moisture is directly involved in the aerosol formation.[4] Furthermore, humid climates increase the likelihood of viruses adhering to airborne particles and correspondingly increase the mortality rate from infectious diseases.[5] Therefore, there is an urgent need to advance filtration technologies to mitigate the hazards of fine particles.

One of the most effective ways to remove particles from air is through filtration.[6,7] Many traditional fiber materials (such as cotton, nylon, polyester, conventional cellulose, and others) are used to fabricate air filters.[8] However, due to the large pore sizes (12–60 μm) of these conventional filter materials, many submicron fine particles can easily penetrate through the fibers, resulting in clogging and reduced filtration efficiency.[9–13] Additionally, as the fine particles build up on the filter, the pressure loss in the airflow also increases.[14]

Compared to conventional filters, nanofiber membranes prepared through electrospinning technology have the advantages of high porosity, micro and nano-channel interconnections, high specific surface area, and good mechanical properties.[15–18] Not only do they have a strong adsorption effect on PM, but the electrospun nanofibers also have a strong interaction with the substrate. Consequently, the nanofiber layer does not fall off when dust is removed from the surface of the filter material.[19–21] Thus, depositing a layer of ultrathin nanofibers on conventional filter materials using electrospinning technology is a viable option to obtain high-performance $PM_{2.5}$ filters.[22] Li *et al.* [23] reported a $PM_{2.5}$ capture efficiency of 99.95% for a composite filter paper prepared by electrospinning poly(vinyl alcohol) (PVA) nanofibers onto a nonwoven polypropylene (PP) substrate using a needle-free electrostatic spinning technique. Patanaik *et al.*[24] electrospun polyethylene oxide (PEO) nanofibers onto nonwoven fabrics and evaluated their long-term stability. However, these composite filters (*e.g.*, PVA and PEO) are hydrophilic and susceptible to water damage, making it challenging to maintain stable long-term particulate filtration efficiency under high humidity conditions.[25]

Electrospun hydrophobic materials such as polyvinylidene fluoride (PVDF) and thermoplastic polyurethane (TPU) can be readily integrated to improve the hydrophobicity of composite filters and extend their useful life.[26,27] Among these, PVDF is highly attractive for its low cost and excellent chemical stability.[28] In addition, the polarity in PVDF promotes the interaction between PM and the nanofibers, resulting in higher PM capture efficiency.[29] However, on the downside, PVDF-based

[a]*College of Engineering Science and Technology, Shanghai Ocean University, Shanghai, 201306, P.R. China*

[b]*Institute of Guizhou Aerospace Measuring and Testing Technology, Guiyang 550009, P.R. China*

[c]*Center for Advanced Electronic Materials and Devices, School of Electronic Information and Electrical Engineering, Shanghai Jiaotong University, Shanghai 200240, P.R. China*

[d]*Zhangjiagang Water Company Limited, Jiangsu, 215600, P.R. China*

[e]*School of Electronics, Information and Electrical Engineering, Shanghai Jiao Tong University, Shanghai 200240, P. R. China*

membranes face specific challenges, such as weak mechanical properties and poor thermal stability, limiting their use.[30] To fix these problems, composite nanofibers can be prepared by incorporating PVDF with other materials. For instance, Chen *et al.*[31] proposed high-performance air filtration membranes consisting of one-dimensional (1D) PVDF nanofibers and two-dimensional (2D) graphene oxide (GO) nanosheets, having good filtration efficiency (99.31%). Additionally, the tensile strength of the GO/PVDF NFMs (nanofiber membranes) was 74.1% higher than that of the pure PVDF NFMs. Zhang *et al.*[32] reported a $PM_{2.5}$ capture was fabricated by introducing an ultra-thin polyvinylidene fluoride (PVDF) nanofibrous layer on the filter materials *via* electrospinning technology, and its long-term filtration and ventilation rate experiments show that the composite filter has stable high filtration efficiency (98.137–96.36%) and ventilation rate. These efforts demonstrated promising mechanical performance; however, the filtration performance and thermal stability of the electrospun nanofibers need further attention. Dai *et al.*[33] showed that incorporating polyimide (PI) into electrospun nanofibers can improve thermal stability along with the mechanical properties of air filtration membranes.

The present study prepares air filtration membranes by incorporating polyimide and graphene oxide into PVDF nanofibers. These PVDF/GO/PI composite NFMs have the advantages of being lightweight and having good permeability, while their adsorption performance and thermal stability are also significantly improved. Compared to the 88.3% $PM_{2.5}$ filtration efficiency and 478 Pa pressure drop of the commercial filter, the filtration efficiency of the PVDF/GO/PI NFM filter is improved to 99.6% while the pressure drop is reduced to 123 Pa. In addition, after heat treatment at 450°Cfor 1 h, the PVDF/GO/PI NFM membrane still retains an excellent removal efficiency of 99.1%. Moreover, the composite membrane possesses superior mechanical properties and cyclic performance, with the filtration efficiency maintained at 99.1% in repeated filtration experiments. In conclusion, PVDF/GO/PI NFM has excellent comprehensive performance and is a new material with great application prospects.

2. Experimental

2.1. Materials

Graphene oxide powder (GO; models: D (GO-P3-FM); layer < 3; sheet size < 10 μm) was purchased from DC(Suzhou) New Materials Science and Technology Co., Ltd., China. Polyvinylidene fluoride (PVDF; $M_w = 80\,000$; CAS No. 24937-79-9) and polyimide powder (PI; $M_w = 50\,000$–$80\,000$; CAS No. 62929-02- 6) was obtained from Shanghai McLean Biochemical Co. Ltd., China. *N*,*N*-Dimethylformamide (DMF; 99.5%; CAS No. 68-12-2) was provided by Aladdin Chemical Reagent Co., China. All the chemicals were used as received without further purification.

2.2. Preparation of the PVDF/GO/PI nanofiber membranes

Initially, 0.0514 g of GO powder was added into 20 mL of DMF and sonicated for 30 min. The dispersion was then added with 10 mL of acetone (keeping the mass ratio of DMF to acetone at 7 : 3) and further sonicated for 30 min. Subsequently, 5.14 g of PVDF powder was slowly added into the mixture with continuous magnetic stirring for 4 h at 45 °C to obtain a homogenous liquid phase. Finally, an appropriate amount of PI powder (0.1028 g, 0.2056 g, 0.3084 g, 0.4112 g) was mixed with the solution and stirred for 12 h at 80 °C for homogenous dispersion. In this way, four different solutions with the mass ratio of PI to PVDF powder being 2%, 4%, 6%, and 8% were obtained. Finally, the solutions were electrospun into PVDF/GO/PI nanofibers under a controlled voltage of 20 kV, the solution injection rate of 2 mL h^{-1}, and the distance between the capillary port and the collector maintained at 16 cm. To obtain nanofiber membranes of the same thickness, the back-and-forth motion of the spinning needle was controlled at 1 m min^{-1} while maintaining the roller speed at 80 rpm. We control the thickness of nanofiber membrane by setting the electrospinning time. For each type of PVDF, PVDF/GO, PVDF/GO/PI membrane, we set five different electrospinning time: 30 min, 60 min, 90 min, 120 min, 150 min. The filtration efficiencies were tested, and the better results were found at about 60 minutes of electrospinning time for these membranes. For comparison, the membranes prepared with 60 min electrospinning time were subsequently used for characterization and performance studies. The electrospun nanofiber films with controlled thickness were finally collected on aluminum foil wrapped around the roller after an optimum electrospinning time. The resulting nanofiber membranes were denoted as PVDF/GO/PI-*x*, where *x* is 2, 4, 6, and 8, corresponding to the composition of the precursor solution.

2.3. Characterization

Field emission scanning electron microscopy (FESEM, Gemini SEM7426, ZEISS) was employed to observe the morphology of the materials. Fourier transform infrared (FTIR) spectra were obtained using a Fourier transform infrared spectrometer (FTIR, Nicolet 6700, Thermo Fisher). The mechanical performance of the materials was evaluated by Dynamic Mechanical Analyzer (DMA, Q850, PerkinElmer). A thermogravimetric analyzer (TGA, Pyris1, PerkinElmer) was used to determine the thermal stability of the materials. The water contact angle of the materials was measured by a droplet shape analyzer (DSA100, Kruss). To evaluate the performance of the material as a membrane, the filtration efficiency was measured using a homemade adsorption device, as shown in Fig. 4a, was used to perform retention tests for $PM_{2.5}$. The contaminant $PM_{2.5}$ was generated by burning incense to simulate actual pollution, and the electrospun nanofibers were utilized as air filtration membranes in the device. A an SDC2501 $PM_{2.5}$ detector was employed to measure the $PM_{2.5}$ concentration difference across the two sides of the membrane, while the pressure drop was determined using a differential pressure meter (AS510).The burning incense was extinguished when the $PM_{2.5}$ concentration difference reached 460 μg m^{-3} and the vacuum filtration pump was then turned on to filter the contaminated air.For testing the adsorption capacity, an airflow rate of 0.2 m s^{-1} was

maintained through a test area of 78.5 cm^2 of the NFMs by adjusting the power of a vacuum pump.

3. Results and discussion

3.1. Material characterization of the PVDF/GO/PI membranes

Fig. 1a depicts the electrospinning process of the nanofibers with the composition of the electrospinning solution shown in Fig. 1b. Three types of solutions were utilized, namely transparent solution 1 containing PVDF and DMF, transparent black solution 2 containing GO, PVDF, and DMF, and transparent gray solution 3 containing GO, PI, PVDF, and DMF.

Fig. 2 shows the diameter distribution and SEM images of the different nanofibers. The statistical analysis (Fig. 2a–c) indicated that the diameters of the PVDF, PVDF/GO, and PVDF/GO/PI-6 nanofibers were all normally distributed. From the highest point of the curves, it can be observed that the fitted values of the diameters of the PVDF, PVDF/GO, and PVDF/GO/PI-6 nanofibers were 359 nm, 448 nm, and 447 nm, respectively. Fiber diameter is solely influenced by electrospinning factors, such as spinning voltage, receiving distance, and the properties of the solution, including viscosity and conductivity. In this study, we controlled the introduction of PI. The difference between the components was not significant. Due to the smaller proportion of PI added, it had less effect on the viscosity and conductivity of the solution, resulting in a smaller influence on the nanofiber diameter during spinning.

Fig. 2d–i shows that the three types of nanofibers exhibited different adsorption characteristics for the same adsorption time. For the PVDF nanofibers, it was found that $PM_{2.5}$ aggregated in a spindle shape, mainly on the nodes, with a few aggregates along the fibers. In the case of PVDF/GO nanofibers, $PM_{2.5}$ was adsorbed in a bead-like shape on the nodes and along the length of the fibers. On the contrary, the PVDF/GO/PI nanofibers adsorbed $PM_{2.5}$ more uniformly in the form of bead chains and an approximate ellipsoidal rather than spindle shape. Moreover, the volume of $PM_{2.5}$ adsorbed on PVDF/GO/PI nanofibers was more significant than that of the PVDF and PVDF/GO nanofibers. The ability of $PM_{2.5}$ particles to aggregate on the nanofibers may be related to dipole moment interactions between the polar surface functional groups on the PVDF nanofibers and the polar surface functional groups of the $PM_{2.5}$ particles. However, localized aggregation at the nodes may be due to the interaction between the adsorbed $PM_{2.5}$ particles. Furthermore, the high concentration of nanofibers at the nodes may contribute to the aggregation of $PM_{2.5}$ particles in those areas. In the case of PVDF/GO/PI nanofibers, $PM_{2.5}$ was uniformly adsorbed on each nanofiber (Fig. 2i). The addition of GO powder introduces more hydrophilic functional groups to the novel electrostatically spun nanofibers, which facilitates the uniform binding of $PM_{2.5}$ particles to the nanofibers. In addition to polyvinylidene fluoride groups, the oxygen-containing groups in graphene oxide exhibit excellent hydrophilicity. This property promotes the uniform adsorption of $PM_{2.5}$ by nanofibers. Since $PM_{2.5}$ is typically a solid or liquid aerosol, the hydrophilicity of the oxygen-containing groups facilitates the adsorption of more water in the gas stream, making adsorption easier to achieve. The large dipole moments of the PI molecules also contribute significantly to the adsorption of PM.

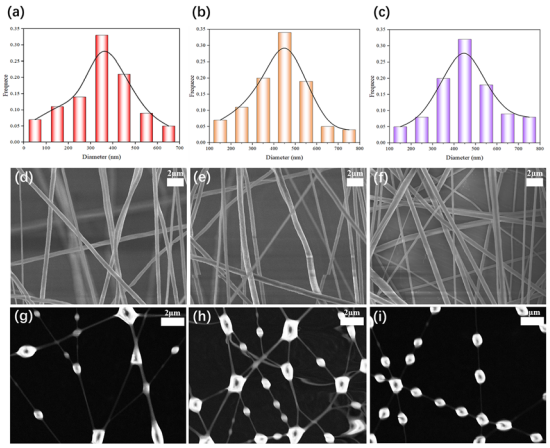

Fig. 2 Diameter statistics of (a) PVDF, (b) PVDF/GO, and (c) PVDF/GO/PI-6 nanofibers. SEM images of the as-prepared (d) PVDF, (e) PVDF/GO, and (f) PVDF/GO/PI-6. SEM images of (g) PVDF, (h) PVDF/GO, and (i) PVDF/GO/PI-6 nanofibers after $PM_{2.5}$ adsorption.

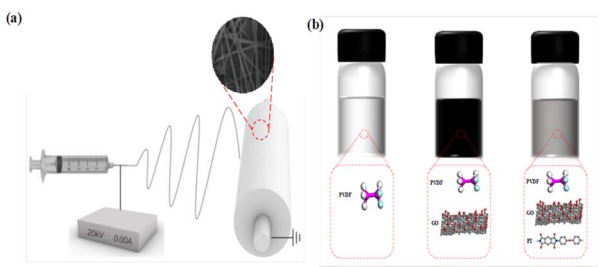

Fig. 1 (a) Fabrication process of electrospinning nanofibers and (b) the compositions of electrospinning solutions.

The adsorption of PM onto PVDF nanofibers depends on the polarity of the nanofibers. However, the adsorption capacity may be limited, resulting in spindle-like adsorption. The addition of GO supplements more hydrophilic functional groups, which allows for better adsorption onto PM containing water. As a result, the adsorption effect is in the form of a bead. After the addition of PI with a large dipole moment, the adsorption capacity is further promoted, resulting in the formation of more sufficient and uniform beads and ellipsoids. Therefore, the adsorption effect is in the form of beads and ellipsoids. The removal efficiency of the polyacrylonitrile/graphene oxide/polyimide nanofibers was further improved compared to that of the pure polyvinylidene fluoride nanofibers and polyvinylidene fluoride/graphene oxide nanofibers.

The functional groups on GO, PI, PVDF, and PVDF/GO/PI were analyzed by FTIR spectroscopy, as shown in Fig. 3a.The infrared spectral spectrum of GO shows absorption peaks at 1672 cm^{-1}, 1384 cm^{-1} and 1066 cm^{-1}, which can be attributed to vibrational stretching of aromatic (C=C) bonds, bending vibration of hydroxyl groups (–OH), and vibrational and stretching of alkoxy (C–O) groups, respectively.[34] Typical

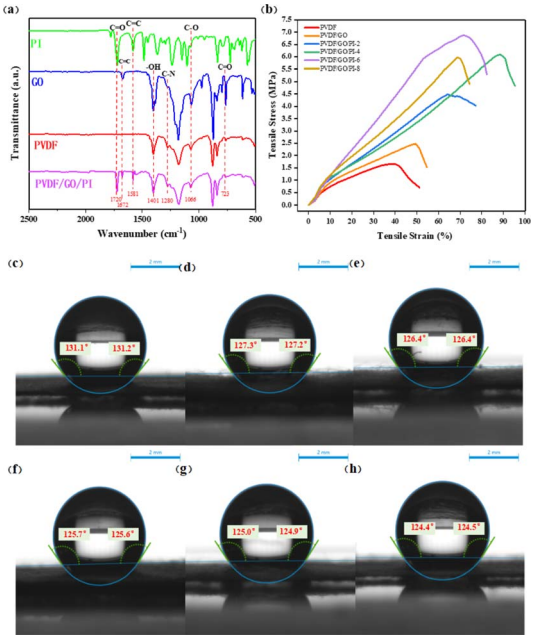

Fig. 3 (a) FTIR spectra of PI, GO, PVDF, and PVDF/GO/PI-6. (b) Stress–strain curves of the various nanofibers. Contact angles of nanofibers membranes composed of (c) PVDF, (d) PVDF/GO, (e) PVDF/GO/PI-2, (f) PVDF/GO/PI-4, (g) PVDF/GO/PI-6, (h) PVDF/GO/PI-8.

absorption peaks in the PVDF spectrum at 1401 cm^{-1}, 1280 cm^{-1}, 1066 cm^{-1}, and 723 cm^{-1} correspond to –OH stretching vibration, C–N stretching vibration, C–O stretching vibration, and C=O bending vibration, respectively.[35] In the PI spectrum, the peaks at 1720 cm^{-1}, 1581 cm^{-1}, 1066 cm^{-1}, and 723 cm^{-1} belong to asymmetric C=O stretching, symmetric C=C stretching, –OH stretching, and C=O bending vibrations in the imide structure, respectively.[36] The FTIR spectrum of PVDF/GO/PI nanofibers is a combination of the GO, PI, and PVDF spectra, indicating the co-existence of all the functional groups in the composite material. Thus, the abundant functional groups on the PVDF/GO/PI nanofibers tended to significantly affect the adsorption of $PM_{2.5}$ due to strong interactions.

Mechanical properties are among the main indices of nanofiber membranes. Experimentally determined stress–strain curves of the PVDF/GO/PI membranes are shown in Fig. 3b. It can be seen that the incorporation of PI has improved the mechanical properties of the PVDF nanofibers (initial tensile strength is nearly 1.5 MPa and elongation is 40%) may be due to the rigid chemical structure of the former polymer. Therefore, with the increase in PI amount, the tensile strength of the PVDF/GO/PI membranes showed an upward trend. Comparing the stress–strain curves, it can be observed that the PVDF/GO/PI-6 had the highest tensile strength (approaching 7 MPa), while the PVDF/GO/PI-4 showed the highest elongation (approaching 90%). Moreover, with the addition of PI, the stiffness of the nanofiber membrane increased significantly, suggesting enhanced resistance of the PVDF/GO/PI nanofiber membranes to mechanical deformation. However, at the same time, the PVDF/GO/PI nanofiber membrane maintained sufficient flexibility. Changes in the hydrophilicity of the membranes were examined in terms of water contact angle, as shown in Fig. 3c–h. These angles were measured to be 131.1°, 127.3°, 126.4°, 125.7°, 125.0°, and 124.4° for pure PVDF, PVDF/GO, PVDF/GO/PI-2, PVDF/GO/PI-4, PVDF/GO/PI-6, and PVDF/GO/PI-8 nanofiber membranes, respectively. The addition of graphene oxide and polyimide thus slightly decreased the water contact angle while the membranes remained hydrophobic.

3.2. Filtration performance of the PVDF/GO/PI membranes

Filtration efficiency is an important performance index to evaluate the suitability of a membrane to retain $PM_{2.5}$. The results, as shown in Fig. 4b, indicate superior performance of the PVDF/GO/PI-6 nanofibers compared to that of PVDF. Fig. 4c shows that the equilibrium filtration efficiency of the commercial membranes (nonwoven fabric), PVDF, PVDF/GO, PVDF/GO/PI-2, PVDF/GO/PI-4, PVDF/GO/PI-6, and PVDF/GO/PI-8 nanofiber membranes were 88.3%, 93.6%, 98.2%, 98.7%, 99.1%, 99.6%, and 98.8%, respectively. There are different types of $PM_{2.5}$ movement, including inertial impact, gravitational settling, and Brownian motion.[37,38] When unpurified air passes through the PVDF nanofibers, larger particles are physically intercepted and adsorbed on the fiber nodes through impact and inertial collision of the fibers. The smaller particles aggregate on the nanofibers due to dipole moment interactions between the polar surface functional groups on the PVDF nanofibers and the $PM_{2.5}$ particles. As stated in Section 3.1, the inclusion of GO and PI increased the number of functional group sites on the nanofibers, allowing for greater adsorption of particulate matter. Additionally, the polarity of the nanofibers was enhanced, resulting in improved adsorption of smaller particulate matter by the PVDF/GO/PI nanofibers. Consequently, the filtration efficiency of the composite nanofibers was improved.

To gain further insight into the filtration efficiency of the membranes, Fig. 4d showcases the filtration efficiency of the different membranes for the first 1000 s. The adsorption rates of

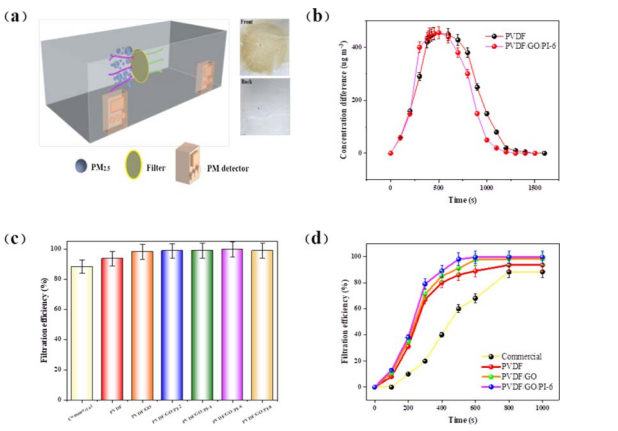

Fig. 4 (a) Schematic illustration of the apparatus used for the purification process and photographs of the front and back sides of the PVDF/GO/PI-6 filter. (b) Concentration difference curves of PVDF and PVDF/GO/PI-6 nanofiber membranes. (c) The filtration efficiency of various nanofibers after reaching the absorption equilibrium. (d) The filtration efficiency curve of the three types of nanofibers for the first 1000 s.

all four fibers increased rapidly over a period of 100–500 s. After 600 s, the adsorption process of the noncommercial membranes gradually reached equilibrium, and the filtration efficiencies converged to a stable value. At any moment from the initial to the equilibrium condition, the filtration efficiency of the PVDF/GO/PI nanofiber membranes remained higher than that of the PVDF but close to the PVDF/GO. Thus, introducing GO and PI significantly improves the filtration efficiency of PVDF nanofiber membranes.

In addition to the filtration efficiency, the pressure drop across the membrane must also be considered for comprehensive performance. The combined parameter of filtration efficiency and pressure drop was evaluated in terms of quality factor (QF). Table 1 summarizes the performance parameters of different nanofiber membranes. The pressure drop of the PVDF/GO/PI nanofiber membranes was significantly lower than that of commercial and pure PVDF nanofiber membranes. The specific surface area and porosity of nanofibers are determined by their diameter distribution. Generally, smaller diameter nanofibers have larger specific surface area and porosity, resulting in lower pressure drop through airflow. Conversely, larger diameter nanofibers have smaller specific surface area and porosity, leading to higher pressure drop.

It is important to note that other factors may also affect pressure drop. The fiber properties and pressure drop presented in Table 1 of this experiment require further analysis. The relationship between pressure drop and fiber diameter observed in the experiment does not align with the theoretical framework outlined above. This inconsistency may be attributed to the following factors: Due to the addition of subsequent materials, the viscosity of the electrospinning solution increased slightly, resulting in an increase in the diameter of the produced nanofibers. However, the addition of new materials may affect the mechanical properties of the nanofibers, which in turn may affect the structural arrangement and distribution of the fiber-forming film. This can lead to an increase in the diameter and distribution of the nanofibers. Thus, the fiber gap was increased, resulting in larger airflow channels and a subsequent reduction in pressure drop. Consequently, the PVDF/GO/PI-6 nanofiber membrane possessed the highest QF (0.0449 Pa^{-1}) among all the tested membranes. The results thus indicated that the PVDF/GO/PI nanofiber membranes had superior comprehensive performance with higher filtration efficiency and lower pressure drop.

Table 1 Filter performance parameters of various nanofibers[a]

Sample	E/%	Δp/Pa	QF/Pa^{-1}
Commercial	88.3	478	0.0046
PVDF	93.6	177	0.0155
PVDF/GO	98.2	143	0.0281
PVDF/GO/PI-2	98.7	137	0.0317
PVDF/GO/PI-4	99.1	129	0.0365
PVDF/GO/PI-6	99.6	123	0.0449
PVDF/GO/PI-8	98.8	132	0.0335

[a] $QF = -\ln(1 - E/100)/\Delta p$,[39] where QF = quality factor, E = filtration efficiency, and Δp = pressure drop.

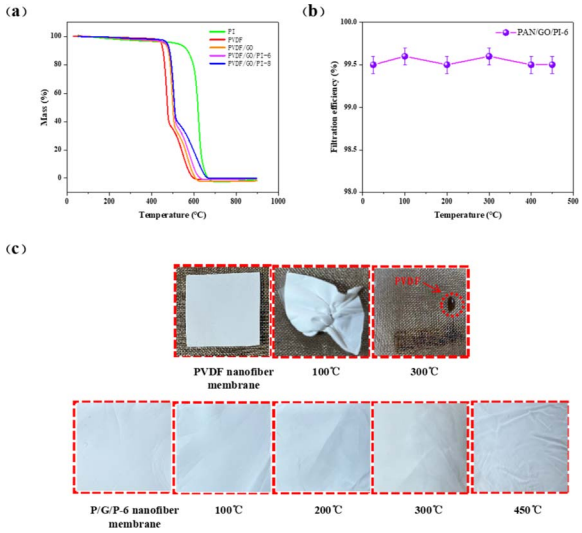

Fig. 5 (a) TGA curves of PI, PVDF, PVDF/GO, PVDF/GO/PI-6 and PVDF/GO/PI-8 nanofibrous membranes. (b) $PM_{2.5}$ filtration efficiency of the PVDF/GO/PI-6 nanofibrous membrane after heat treatment at different temperatures for 1 h. (c) Photographs of PVDF nanofiber membrane and P/G/P-6 nanofiber membrane treated at different temperatures.

3.3. Thermal stability of the PVDF/GO/PI nanofiber membranes

To explore the thermal stability of the membranes at high temperatures, thermogravimetric spectroscopy is usually performed. Fig. 5a shows the thermograms of PI, PVDF, and PVDF/GO/PI nanofibers from room temperature to 900 °C obtained under air atmosphere. Thermal degradation of the polyimide was observed at 600 °C, while that of PVDF occurred between 300–440 °C. On the contrary, the PVDF/GO/PI composite experienced significant thermal degradation at around 450 °C.

To qualify the thermal stability, the PVDF/GO/PI nanofiber membranes were heat-treated at different temperatures (100 °C, 200 °C, 300 °C, 400 °C, 450 °C) for 1 h, and their filtration efficiency was determined. Fig. 5b shows appreciably high filtration efficiency of the PVDF/GO/PI-6 nanofiber membrane after heat treatment at different temperatures, confirming its thermal stability of up to 450 °C. The photographs of pure PVDF air filtration material and PVDF/GO/PI-6 treated at different temperatures for 1 hour are shown in Fig. 5c. The pure PVDF air filtration material exhibited melting after treatment at 300 °C, whereas PVDF/GO/PI-6 did not show significant shrinkage after treatment at 450 °C, indicating superior thermal stability. This study thus demonstrated that the PVDF/GO/PI nanofiber membranes have high filtration efficiency and remarkable thermal stability compared to the previous literature.[40–42]

4. Conclusions

In this study, PVDF/GO/PI nanofiber membranes for air filtration were prepared using the electrospinning method. Compared with pure PVDF and PVDF/GO nanofiber membranes, the air filters composed of PVDF/GO/PI nanofibers

were more effective in trapping $PM_{2.5}$ pollutants. The PVDF/GO/PI nanofiber membranes not only possessed a high filtration efficiency (99.6%) and a low pressure drop (123 Pa) but also had excellent thermal stability (450 °C) and superior mechanical properties (7 MPa). It is anticipated that the PVDF/GO/PI nanofiber membranes interacted with $PM_{2.5}$ and effectively adsorbed the particles, leading to high filtration efficiency. Moreover, the high thermal stability of the PVDF/GO/PI nanofiber membranes comes from the unique molecular structure of the polyimide component. Thus, considering these advantages, the prepared PVDF/GO/PI composite nanofibrous membranes can find a wide range of applications in various industrial and civil fields.

Author contributions

Hangdong Chen: conceptualization, visualization, formal analysis, writing – original draft, writing – review & editing. Xun Sun: methodology, formal analysis, writing – review & editing. Ying Wang: methodology, writing – review & editing. Lixian Shi: investigation, validation. Xuan Liu: project administration, funding acquisition, supervision. Nantao Hu: funding acquisition, supervision.

Conflicts of interest

There are no conflicts to declare.

Acknowledgements

This project is supported by the National Natural Science Foundation of China (51005145, 51075258), Medical-Engineering Cross-Fund of Shanghai Jiao Tong University (YG2021ZD27, YG2022ZD025), Interdisciplinary Program of Shanghai Jiao Tong University (No. YG2022QN101), and the Key Laboratory for Thin Film and Microfabrication Technology of the Ministry of Education, Shanghai Jiaotong University.

Notes and references

1 M. Brauer, G. Hoek, H. A. Smit, J. C. de Jongste, J. Gerritsen, D. S. Postma, M. Kerkhof and B. Brunekreef, Air pollution and development of asthma, allergy and infections in a birth cohort, *Eur. Respir. J.*, 2007, **29**, 879–888.

2 W. Jung, J. S. Lee, S. Han, S. H. Ko, T. Kim and Y. H. Kim, An efficient reduced grapheneoxide filter for $PM_{2.5}$ filtration, *J. Mater. Chem. A*, 2018, **6**, 16975–16982.

3 Y. Zhang, S. Yuan, X. Feng, H. Li, J. Zhou and B. Wang, Preparation of nanofibrous metal–organic framework filters for efficient air pollution control, *J. Am. Chem. Soc.*, 2016, **138**, 5785–5788.

4 (*a*) Y. Li, X. Yin, J. Yu and B. Ding, Electrospun nanofibers for high-performance air filtration, *Compos. Commun.*, 2019, **15**, 6–19; (*b*) X. Zhao, S. Wang, X. Yin, J. Yu and B. Ding, Slip-effect functional air filter for efficient purification of $PM_{2.5}$, *Sci. Rep.*, 2016, **6**, 35472.

5 A. Barhoum, K. Pal, H. Rahier, H. Uludag, I. S. Kim and M. Bechelany, Nanofibers as new-generation materials: From spinning and nano-spinning fabrication techniques to emerging applications, *Appl. Mater. Today*, 2019, **17**, 1–35.

6 A. C. C. Bortolassi, S. Nagarajan, B. D. Lima, V. G. Guerra, M. L. Aguiar, V. Huon, L. Soussan, D. Cornu, P. Miele and M. Bechelany, Efficient nanoparticles removal and bactericidal action of electrospun nanofibers membranes for air filtration, *Mater. Sci. Eng., C*, 2019, **102**, 718–729.

7 W. Hua, T. Zhang, S. Ding and X. Wang, A novel cost-effective PAN/CNS nanofibrous membranes with rich carboxyl groups for high efficient adsorption of Lanthanum(III) ions, *Sep. Purif. Technol.*, 2021, **259**, 118216.

8 Y. Bian, R. Wang, S. H. Ting, C. Chen and L. Zhang, Electrospun SF/PVA nanofiber filters for highly efficient $PM_{2.5}$ capture, *IEEE Trans. Nanotechnol.*, 2018, **17**, 934–939.

9 J. Yu, C. Zhang, W. Wu, Y. Cai and Y. Zhang, Nodes-connected silicon-carbon nanofibrous hybrids anodes for lithium-ion batteries, *Appl. Surf. Sci.*, 2021, **548**, 148944.

10 X. Zhao, Y. Li, T. Hua, P. Jiang, X. Yin, J. Yu and B. Ding, Cleanable air filter transferring moisture and effectively capturing $PM_{2.5}$, *Small*, 2017, **13**, 1603306.

11 G. Gong, K. Gao, J. Wu, N. Sun, C. Zhou, Y. Zhao and L. Jiang, A highly durable silica/polyimide superhydrophobic nanocomposite film with excellent thermal stability and abrasion-resistant performance, *J. Mater. Chem. A*, 2015, **3**, 713–718.

12 L. Yao, X. Dong, C. Zhang, N. Hu and Y. Zhang, Metal oxide nanoprism-arrays assembled in N-doped carbon foamy nanoplates that have efficient polysulfideretention for ultralong-cycle-life lithium-sulfur batteries, *J. Mater. Chem. A*, 2018, **6**, 11260–11269.

13 V. Kadam, I. L. Kyratzis, Y. B. Truong, J. Schutz, L. Wang and R. Padhye, Electrospun bilayer nanomembrane with hierarchical placement of bead-on-string and fibers for low resistance respiratory air filtration, *Sep. Purif. Technol.*, 2019, **224**, 247–254.

14 M. Karakoti, R. Jangra, S. Pandey, P. S. Dhapola, S. Dhali, S. Mahendia, P. K. Singh and N. G. Sahoo, Binder-free reduced graphene oxide as electrode material for efficient supercapacitor with aqueous and polymer electrolytes, *High Perform. Polym.*, 2020, **32**, 175–182.

15 H. Zhao, N. Deng, W. Kang, Z. Li, G. Wang and B. Cheng, Highly multiscale structural poly(vinylidene fluoridehexafluoropropylene)/poly-*m*-phenyleneisophthalamide separator with enhanced interface compatibility and uniform lithium-ion flux distribution for dendrite-proof lithium-metal batteries, *Energy Storage Mater.*, 2020, **26**, 334–348.

16 J. Ren, Y. C. Woo, M. Yao, S. Lim, L. D. Tijing and H. K. Shon, Nanoscale zero-valent iron (nZVI) immobilization onto graphene oxide (GO)-incorporated electrospun polyvinylidene fluoride (PVDF) nanofiber membrane for groundwater remediation *via* gravity-driven membrane filtration, *Sci. Total Environ.*, 2019, **688**, 787–796.

17 Z.-X. Huang, X. Liu, X. Zhang, S.-C. Wong, G. G. Chase, J.-P. Qu and A. Baji, Electrospun polyvinylidene fluoride

containing nanoscale graphite platelets as electret membrane and its application in air filtration under extreme environment, *Polymer*, 2017, **131**, 143–150.

18 A. M. Elsaid and M. S. Ahmed, Indoor air quality strategies for air-conditioning and ventilation systems with the spread of the global coronavirus (COVID-19) epidemic: improvements and recommendations, *Environ. Res.*, 2021, **199**, 111314.

19 M. Ahmadzadeh, E. Farokhi and M. Shams, Investigating the effect of air conditioning on the distribution and transmission of Covid-19 virus particles, *J. Cleaner Prod.*, 2021, **316**(128147).

20 S. Han, J. Kim and S. H. Ko, Advances in air filtration technologies: structure-based and interaction-based approaches, *Mater. Today Adv.*, 2021, **9**(100134).

21 T. Kurabuchi, M. Ogata, M. Otsuka and N. Kagi, Operation of air-conditioning and sanitary equipment for SARS-CoV-2 infectious disease control, *Jpn. Arch. Rev.*, 2021, **4**(4), 608–620.

22 H. Zhang, D. Hines and D. L. Akins, Synthesis of a nanocomposite composed of reduced graphene oxide and gold nanoparticles, *Dalton Trans.*, 2014, **43**, 2670–2675.

23 Y. Ren, T. Huo, Y. Qin and X. Liu, Preparation of flame retardant polyacrylonitrile fabric based on sol-gel and layer-by-layer assembly, *Materials*, 2018, **11**, 483.

24 A. Patanaik, V. Jacobs and R. D. Anandjiwala, Performance evaluation of electrospun nanofibrous membrane, *J. Membr. Sci.*, 2010, **352**(1–2), 136–142.

25 C. Zhang, L. Yao, Z. Yang, E. S.-W. Kong, X. Zhu and Y. Zhang, Graphene oxide modified polyacrylonitrile nanofibrous membranes for efficient air filtration, *ACS Appl. Nano Mater.*, 2019, **2**, 3916–3924.

26 Z. Wang, C. Zhao and Z. Pan, Porous Bead-on-String Poly(lactic acid) Fibrous Membranes for Air Filtration, *J. Colloid Interface Sci.*, 2015, **441**, 121–129.

27 Y. Liu, M. Park, B. Ding, J. Kim, M. El-Newehy, S. S. Al-Deyab and H.-Y. Kim, Facile Electrospun Polyacrylonitrile/Poly(acrylic acid) Nanofibrous Membranes for High Efficiency Particulate Air Filtration, *Fibers Polym.*, 2015, **16**, 629–633.

28 X. Zhao, Y. Li, T. Hua, P. Jiang, X. Yin, J. Yu and B. Ding, Cleanable Air Filter Transferring Moisture and Effectively Capturing $PM_{2.5}$, *Small*, 2017, **13**, 1603306.

29 N. Hu, Y. Wang, J. Chai, R. Gao, Z. Yang, E. S.-W. Kong and Y. Zhang, Gas Sensor Based on P-phenylenediamine Reduced Graphene Oxide, *Sens. Actuators, B*, 2012, **163**, 107–114.

30 C.-S. Wang and Y. Otani, Removal of Nanoparticles from Gas Streams by Fibrous Filters: A Review, *Ind. Eng. Chem. Res.*, 2013, **52**, 5–17.

31 Y. Chen, S. Zhang, S. Cao, S. Li, F. Chen, S. Yuan, C. Xu, J. Zhou, X. Feng, X. Ma and B. Wang, Roll-to-roll production of metal–organic framework coatings for particulate matter filtration, *Adv. Mater.*, 2017, **29**, 1606221.

32 H. Zhang, D. Hines and D. L. Akins, Synthesis of A Nanocomposite Composed of Reduced Graphene Oxide and Gold Nanoparticles, *Dalton Trans.*, 2014, **43**, 2670–2675.

33 H. Dai, X. Liu, C. Zhang, K. Ma and Y. Zhang, Electrospinning Polyacrylonitrile/Graphene Oxide/Polyimide nanofibrous membranes for High-efficiency $PM_{2.5}$ filtration, *Sep. Purif. Technol.*, 2021, **276**, 119243, DOI: **10.1016/j.seppur.2021.119243**.

34 P. Li, C. Wang, Y. Zhang and F. Wei, Air Filtration in the Free Molecular Flow Regime: A Review of High-Efficiency Particulate Air Filters Based on Carbon Nanotubes, *Small*, 2014, **10**, 4543–4561.

35 J. Xiao, J. Liang, C. Zhang, Y. Tao, G.-W. Ling and Q.-H. Yang, Advanced Materials for Capturing Particulate Matter: Progress and Perspectives, *Small Methods*, 2018, **2**, 1800012.

36 X. Zhao, S. Wang, X. Yin, J. Yu and B. Ding, Slip-Effect Functional Air Filter for Efficient Purification of $PM_{2.5}$, *Sci. Rep.*, 2016, **6**, 35472.

37 M. Chen, Q. Hu, X. Wang and W. Zhang, A review on recent trends of the antibacterial nonwovens air filter materials: Classification, fabrication, and application, *Sep. Purif. Technol.*, 2024, **330**, 125404, DOI: **10.1016/j.seppur.2023.125404**.

38 Z. Mou, J. Li, C. Liu, Y. Tan, Z. Yan, Y. Liu, Z. Lin, X. Chen and T. Duan, Efficient and multi-functional integrated iodine adsorption air filter for iodine aerosol purification, *Sep. Purif. Technol.*, 2024, **341**, 126895, DOI: **10.1016/j.seppur.2024.126895**.

39 S. Luo, L. Peng, Y. Xie, X. Cao, X. Wang, X. Liu, T. Chen, Z. Han, P. Fan, H. Sun, Y. Shen, F. Guo, Y. Xia, K. Li, X. Ming and C. Gao, *Nano–Micro Lett.*, 2023, **15**, 61, DOI: **10.1007/s40820-023-01032-6**.

40 R. Zhang, C. Liu, P.-C. Hsu, C. Zhang, N. Liu, J. Zhang, H. R. Lee, Y. Lu, Y. Qiu, S. Chu and Y. Cui, Nanofiber air filters with high-temperature stability for efficient $PM_{2.5}$ removal from the pollution sources, *Nano Lett.*, 2016, **16**, 3642–3649.

41 J. Li, D. Zhang, T. Yang, S. Yang, X. Yang and H. Zhu, Nanofibrous Membrane of Graphene Oxide-in-Polyacrylonitrile Composite with Low Filtration Resistance for The Effective Capture of $PM_{2.5}$, *J. Membr. Sci.*, 2018, **551**, 85–92.

42 Y. Wen, Q. Hu, X. Wang, W. Zhang and M. Chen, Electrospun Poly(*m*-phenyleneisophthalamide)/TiO_2 Nanofiber Membranes for Particulate Matter Removal under High-Temperature Conditions, *ACS Appl. Polym. Mater.*, 2024, **6**(3), 1633–1644, DOI: **10.1021/acsapm.3c02355**.